PHYSICAL REVIEW B VOLUME 32, NUMBER 6 15 SEPTEMBER 1985

Plasmon structure in the appearance-potential spectroscopy of metals

Russell Patrick and Shyamalendu M. Bose
Department of Physics and Atmospheric Science, Drexel University, Philadelphia, Pennsylvania 19104

Pierre Longe
Institut de Physique, B5, Université de Liège, Sart-Tilman, B-4000 Liège, Belgium
(Received 20 August 1984; revised manuscript received 16 May 1985)

The effect of plasmon production on the appearance-potential spectra (APS) of simple metals has been calculated in the framework of the many-body perturbation theory. Numerical results are presented for the $2p$ and $1s$ APS of aluminum. In the $2p$ spectrum the plasmon contributes very weakly (beginning with near-zero slope) at the threshold energy for plasmon production $E_{\rm th}(\omega_p^0)=2E_F+\omega_p^0-E_c$ (E_F, ω_p^0, and E_c being the Fermi energy, zero-momentum plasmon frequency, and energy of the core state, respectively). In the $1s$ spectrum, however, there is a finite contribution (beginning with a finite slope) at this threshold. In both $2p$ and $1s$ derivative spectra a structure appears in the form of an inflection in slope of the intensity at the energy $E_{\rm th}(\omega_p(q_c))=2E_F+\omega_p(q_c)-E_c$, where $\omega_p(q_c)$ is the highest frequency for plasmon production. The significance of this energy $E_{\rm th}(\omega_p(q_c))$ is that it is the lowest energy at which the plasmon production by the two final-state electrons, located above the Fermi level, becomes real. A structure also occurs in the $1s$ derivative spectrum at $E_{\rm th}(\omega_p^0)$ as a steep rise, while there is no significant structure at this energy in the $2p$ derivative spectrum. The calculated structures in the derivative spectra appear to be present in the currently available experimental APS of Al.

I. INTRODUCTION

In the appearance-potential spectroscopy (APS) experiment, a fast electron (100—1000 eV) is bombarded on a solid surface. After an inelastic collision with a core-level electron, the system in question is left in a final state consisting of a core hole and two electrons above the Fermi level in the conduction band. What is measured is the x-ray intensity when the core level deexcites, as a function of energy of the incident electron. This intensity spectrum is thus proportional to the number of excited core states per unit time, the object of our many-body study.

The plasmon satellites in the APS spectra of solids have been studied both experimentally and theoretically.[1–5] The observed APS spectrum of graphite[1] shows large peaks separated by an energy of 6.8 eV, a value close to the plasmon loss energy for graphite (7 eV). For simple metals, Andersson and Nyberg[2] have measured the Al $1s$ spectrum, and Nilsson and Kanski[3] have measured the $1s$ and $2p$ spectra for Al, Mg, and Be. In all these cases, structures have been found resembling plasmon oscillations, but in each spectra it is difficult to differentiate between plasmon peaks and variations in the density of states due to band-structure effects. However, by graphically differentiating the spectrum, Andersson and Nyberg found a pronounced peak around 15.5 eV above threshold. They attribute this structure to the excitation of a plasmon in the medium.

Theoretically, Chang and Langreth[4] have studied the APS spectrum associated with the production of a plasmon and found it to be of the same order of magnitude as that found in x-ray photoemission spectra (XPS). In Laramore's paper,[5] plasmon emission up to the first order (one-plasmon emission) have been considered and he derives an approximate expression for the intensity of the plasmon satellite. These studies, however, do not consider the dispersion or attenuation of the plasmon, and Ref. 4 does not take into account the recoil of an electron after the emission of a plasmon. They also do not evaluate the line shape of the plasmon band numerically.

In this paper we will concern ourselves with the plasmon satellites in the APS spectra of simple metals in the presence of plasmon dispersion and the recoil of the electron. Inclusion of these effects will definitely lower the strength of the plasmon satellite and give it a width corresponding to the dispersion of the plasmon. The dispersion relation for the plasmon frequency $\omega_p(q)$ used in this paper is a sixth-order polynomial first derived by Glick and Ferrell,[6] with an eighth-order correction term[7] introduced to obtain the exact plasmon cutoff frequency $\omega_p(q_c)$. The only parameters the metal in question will have are the radius parameter r_s and the core-level energy E_c. The electron-electron interaction effects will be calculated in the random-phase approximation (RPA), describing the polarization in an electron gas.

We will only consider the bulk plasmon, thereby ignoring any surface plasmons in our model. The only role the surface will have in our model will be to introduce a time τ which is the time the incident electron travels in the metal before exciting a core-level state.

There are a few different ways of losing energy due to plasmon production in the APS process. The incident electron can excite a plasmon, this process being an extrinsic one in that the momentum and energy of the system are conserved. The polarization of the conduction band due to the creation of a core hole (which acts like an

impurity) can excite the so-called intrinsic plasmons. The two final-state electrons can also excite intrinsic plasmons.[8,9] Furthermore, there can be interference between any two of the above-mentioned processes, which would reduce the total plasmon contribution, especially in the region close to the threshold. The threshold region corresponds to the case where both the final-state electrons lie close to the Fermi level.

In the next section we will formulate the problem, using an S- and T-matrix approach, which was first proposed by Chastenet and Longe[8] and later used by Bose *et al.*[9] to describe the x-ray photoemission spectra of simple metals. The last section will give numerical results for the $1s$ and $2p$ spectra of Al and a discussion.

II. FORMULATION

Let us consider an incident electron, having wave vector $\mathbf{k}$ and energy $\epsilon_k = k^2/2m$, pointing in a small element $\Delta\mathbf{k}$. The electron enters a semi-infinite metal normally at $z=0$, where the metal extends between $z=0$ and $z=-\infty$.

The strength of the main band ($n=0$) and one-plasmon process ($n=1$) can be written as[8]

$$I_n(\epsilon_k) = \int_{-\infty}^{0} dz\, \rho(z) J_n(z,\epsilon_k) , \\ = v_T \int_0^{\infty} d\tau \rho(\tau) J_n(\tau,\epsilon_k) , \tag{1}$$

where $z=-v_T\tau$ (v_T being the incident electron velocity) and $\rho(z)$ is the density of core-hole states, which we will assume to be a constant in our calculations. $J_n(\tau,\epsilon_k)$ is the probability per unit time that the incident electron with energy ϵ_k travels for a time τ and then excites a core level of energy E_c. $J_n(\tau,\epsilon_k)$ is related to the S matrix by the time-dependent golden rule,

$$J_n(\tau,\epsilon_k) = \frac{n!}{2\pi t_0 N} \sum_f |S_n(\tau,\epsilon_k)|^2 , \tag{2}$$

where

$$\sum_f = \Delta k \sum_{p_1} \sum_{p_2} \Theta(p_1 - k_F)\Theta(p_2 - k_F) \sum_q \Theta(q_c - q) \tag{3}$$

is the sum over all final states, t_0 is the observation time, and N is the normalization constant insuring conservation of the incident electron number and is given by

$$\int_{E_F}^{\epsilon_k + E_c} d\epsilon_k \sum_n J_n(\tau,\epsilon_k) = 1 . \tag{4}$$

Note that to ensure a proper APS process, the sum over the final electron states in (3) must be greater than the Fermi momentum and the plasmon momentum can only go up to the cutoff $q_c \approx m\omega_p^0/k_F$.[10] In the RPA, this is the maximum wave number for collective excitations. Beyond this wave-number plasmon production is heavily damped as the plasmon dispersion line merges into the region of single-particle excitations.

Diagrams that describe the APS matrix elements S_n for the zeroth-order (main band) and one-plasmon processes are shown in Figs. 1 and 2. In these diagrams, a single line pointing up represents a conduction electron; a double line pointing down, a core hole; and a wavy line, the plasmon excitation. As shown in Fig. 2, the incident electron enters the metal at time $t-\tau$, and the core hole is created at time t.

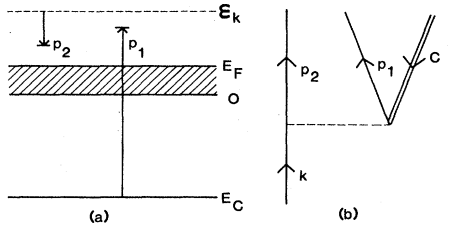

FIG. 1. (a) Schematic representation of the basic APS process in a simple metal. (b) Feynman diagram corresponding to the basic APS process.

For the main band, the zeroth-order matrix element (no plasmon) of the S matrix can be written as

$$S_0 = A \int dt\, g(t) e^{-i(\epsilon_k + E_c - \epsilon_{p_1} - \epsilon_{p_2})t} , \tag{5}$$

with the labels shown in Fig. 1. In (5), $g(t)$ is the adiabatic function[12] for switching on the Coulomb potential

$$g(t) = \begin{cases} 1, & |t| < t_0/2 \\ 0, & |t| > t_0/2 \end{cases} \tag{6}$$

and A is the transition probability amplitude between initial and final states

$$\langle p_1 p_2 | V | kC \rangle , \tag{7}$$

where V is the bare Coulomb interaction. Various authors[4,5] have shown that the momentum dependence of A is weak in the energy range of our interest, and hence A will be considered constant.

Putting (5) into (2) and using an approximation for large t (Ref. 11)

$$\left| \int dt\, g(t) e^{i\nu t} \right|^2 = 2\pi t_0 \delta(\nu) , \tag{8}$$

we have

$$J_0(\tau,\epsilon_k) = \frac{|A|^2 \Delta k}{N} \sum_{p_1\,(>k_F)} \sum_{p_2\,(>k_F)} \delta(\epsilon_k + E_c - \epsilon_{p_1} - \epsilon_{p_2}) , \tag{9}$$

where (3) has been used. The normalization constant N

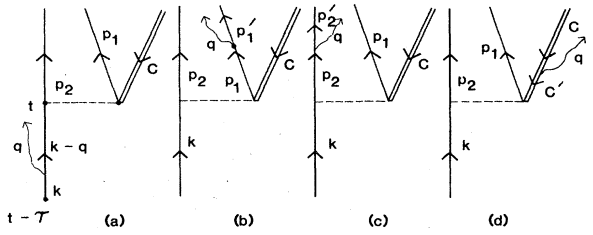

FIG. 2. (a) Diagrams describing the APS S matrix for the zeroth-order (main band) and one-plasmon processes.

must satisfy the sum rule (4) as has been discussed in detail in several publications related to photoemission.[8,9] As in the photoemission case, N will be approximated by

$$N=\exp[\Gamma^*(\epsilon_k)\tau] ,$$

where

$$\Gamma^*(\epsilon_k)=\pi \sum_{q\ (<q_c)} V(q)\omega_p(q)\delta(\epsilon_{|\mathbf{k}+\mathbf{q}|}-\epsilon_k-\omega_p(q)) .$$

This approximation is related to the extrinsic contribution in the T-matrix formalism, the only term explicitly dependent on the time τ of the APS process. The other terms left out of the normalization factor N are not τ dependent and only weakly dependent on the incident energy ϵ_k, and hence do not play any essential role in determining the shape of the intensity of the APS.

Using the normalization condition N and Eq. (1) we have for the main band intensity

$$I_0(\epsilon_k)=\frac{|A|^2\Delta k v_T}{\Gamma^*(\epsilon_k)} \sum_{p_1\ (>k_F)} \sum_{p_2\ (>k_F)} \delta(\epsilon_k+E_c-\epsilon_{p_1}-\epsilon_{p_2}). \tag{10}$$

Since there is no angular dependence, in (10) we can change it to an energy integral,

$$I_0(\epsilon_k)=\frac{|A|^2\Delta k(2m)^3 v_T}{\Gamma^*(\epsilon_k)(2\pi)^4} \int_{E_F}^{\infty} d\epsilon_{p_1} \int_{E_F}^{\infty} d\epsilon_{p_2}(\epsilon_{p_1}\epsilon_{p_2})^{1/2} \times\delta(\epsilon_k+E_c-\epsilon_{p_1}-\epsilon_{p_2}) . \tag{11}$$

Note that this is just the self-convolution of the unoccupied density of states for the free-electron theory of metals. Performing the energy integrals we now have the normalized main band intensity function in dimensionless units as

$$I_0(x_0)\sim\frac{1}{\Gamma^*(z)}\left[\left[\frac{x_0-2}{2}\right](x_0-1)^{1/2} + (x_0/2)^2\sin^{-1}(1-2/x_0)\right] , \tag{12}$$

where $z=k/k_F$ and $x_0=(\epsilon_k+E_c)/E_F$.

For the one-plasmon process, the S-matrix elements (see Fig. 2) can be written as

$$S_a=A \sum_{k'\ (>k_F)} U_{kk'} \int_{-\infty}^{\infty} dt\, g(t) e^{i(\epsilon_{k'}+E_c-\epsilon_{p_1}-\epsilon_{p_2})t} \int_{t-\tau}^{t} dt' g(t') e^{-i[\epsilon_{k'}+\omega_p(q)-\epsilon_k]t} , \tag{13}$$

$$S_b=A \sum_{p_1'\ (>k_F)} U_{p_1p_1'} \int_{-\infty}^{\infty} dt\, g(t) e^{i(\epsilon_k+E_c-\epsilon_{p_1'}-\epsilon_{p_1})t} \int_{t}^{\infty} dt' g(t') e^{-i[\epsilon_{p_1}+\omega_p(q)-\epsilon_{p_1'}]t'} , \tag{14}$$

$$S_c=A \sum_{p_2'\ (>k_F)} U_{p_2p_2'} \int_{-\infty}^{\infty} dt\, g(t) e^{i(\epsilon_k+E_c-\epsilon_{p_1}-\epsilon_{p_2'})t} \int_{t}^{\infty} dt' g(t') e^{-i[\epsilon_{p_2}+\omega_p(q)-\epsilon_{p_2'}]t'} , \tag{15}$$

$$S_d=-A \sum_{C'} U_{CC'} \int_{-\infty}^{\infty} dt\, g(t) e^{i(\epsilon_k+E_c-\epsilon_{p_1}-\epsilon_{p_2})t} \int_{t}^{\infty} dt' g(t') e^{i[E_c-\omega_p(q)-E_{c'}]t'} , \tag{16}$$

where U is the transition matrix for exciting a plasmon

$$U_{ll'}=\int d\mathbf{x}\,\bar{u}_l(\mathbf{x})C(q)W_q(\mathbf{x})u_l'(\mathbf{x}) , \tag{17}$$

with

$$C(q)=[\omega_p(q)V(q)/2]^{1/2} \tag{18}$$

being the plasmon coupling constant, W_q the plasmon wave, and $u_l(\mathbf{x})$ the conduction-band state [or core state in the case of (16)]. For plane-wave states, (17) can be written as

$$U_{ll'}=[\omega_p(q)V(q)/2]^{1/2}\delta_{l',l-\mathbf{q}} , \tag{19}$$

which insures conservation of momentum at the vertices.

In our simple metal the core hole has no structure and therefore can absorb an infinite amount of momentum (no recoil).

The core structure factor in (17)

$$\int d\mathbf{x}\,\bar{u}_C(\mathbf{x})W_q(\mathbf{x})u_{C'}(\mathbf{x})$$

is equal to 1 at $q=0$ and is a slowly varying function of q. As was done in a previous paper on Auger spectroscopy,[12] we will set this factor to 1. Thus for the core excitation of a plasmon, (17) becomes

$$U_{CC'}=[\omega_p(q)V(q)/2]^{1/2}\delta_{CC'} , \tag{20}$$

which will be used in (16). Putting in the appropriate U terms and performing the t' integration, the total first-order S matrix becomes

$$S_1=iA\left[\frac{\omega_p(q)V(q)}{2}\right]^{1/2} \int_{-\infty}^{+\infty} dt\, g(t) e^{i(\omega-\omega_p(q)-\epsilon_{p_1}-\epsilon_{p_2})t} \times\left[\frac{1-e^{i(\omega_p(q)-\epsilon_k+\epsilon_{|\mathbf{k}-\mathbf{q}|})\tau}}{\omega_p(q)-\epsilon_{\mathbf{k}}+\epsilon_{|\mathbf{k}-\mathbf{q}|}} - \frac{\Theta(|\mathbf{p}_1+\mathbf{q}|-k_F)}{\omega_p(q)+\epsilon_{p_1}-\epsilon_{|\mathbf{p}_1+\mathbf{q}|}} - \frac{\Theta(|\mathbf{p}_2+\mathbf{q}|-k_F)}{\omega_p(q)+\epsilon_{p_2}-\epsilon_{|\mathbf{p}_2+\mathbf{q}|}} + \frac{1}{\omega_p(q)}\right] . \tag{21}$$

As with the main band calculation, the first-order intensity function can now be written as

$$I_1(\epsilon_k)=|A|^2\Delta k v_T\int\frac{d\tau}{N}\sum_{p_1>(k_F)}\sum_{p_2>(k_F)}\sum_{q<(q_c)}\delta(\epsilon_k+E_c-\omega_p(q)-\epsilon_{p_1}-\epsilon_{p_2})\left[\frac{\omega_p(q)V(q)}{2}\right]$$
$$\times\left|\frac{1-e^{-i[\epsilon_k-\epsilon_{|\mathbf{k}-\mathbf{q}|}-\omega_p(q)]\tau}}{\epsilon_k-\epsilon_{|\mathbf{k}-\mathbf{q}|}-\omega_p(q)}+\frac{\Theta(|\mathbf{p}_1+\mathbf{q}|-k_F)}{\omega_p(q)+\epsilon_{p_1}-\epsilon_{|\mathbf{p}_1+\mathbf{q}|}}\right.$$
$$\left.+\frac{\Theta(|\mathbf{p}_2+\mathbf{q}|-k_F)}{\omega_p(q)+\epsilon_{p_2}-\epsilon_{|\mathbf{p}_2+\mathbf{q}|}}-\frac{1}{\omega_p(q)}\right|^2. \tag{22}$$

In calculating (22), we use an approximation for large τ,

$$\frac{4\sin^2(\nu\tau/2)}{\nu^2}=2\pi\tau\delta(\nu),\quad\frac{4\sin^2(\nu\tau/2)}{\nu}=\mathrm{P}\frac{2}{\nu}, \tag{23}$$

where P is the principal part. Each of the ten terms in (22) can be represented by a closed diagram as shown in Fig. 3.

Figure 3(a) represents the incident electron exciting a real plasmon (extrinsic), and from (22) the intensity function is written as

$$I_1^e(\epsilon_k)=\frac{|A|^2\pi\Delta k v_T}{[\Gamma^*(\epsilon_k)]^2(2\pi)^9}\int_{|\mathbf{p}_1|>k_F}d^3p_1\int_{|\mathbf{p}_2|>k_F}d^3p_2\int_{|\mathbf{q}|<q_c}d^3q\,\delta(\epsilon_k+E_c-\omega_p(q)-\epsilon_{p_1}-\epsilon_{p_2})$$
$$\times V(q)\omega_p(q)\delta(\epsilon_k-\epsilon_{|\mathbf{k}-\mathbf{q}|}-\omega_p(q)). \tag{24}$$

Figure 3(b) represents an intrinsic process where the core hole polarizes the conduction band, exciting a virtual plasmon. This intensity is written as

$$I^i_{\mathrm{1core}}(\epsilon_k)=\frac{|A|^2\Delta k v_T}{\Gamma^*(\epsilon_k)(2\pi)^9}\int_{|\mathbf{p}|>k_F}d^3p_1\int_{|\mathbf{p}_2|>k_F}d^3p_2\int_{|\mathbf{q}|<q_c}d^3q\frac{V(q)}{2\omega_p(q)}\delta(\epsilon_k+E_c-\omega_p(q)-\epsilon_{p_1}-\epsilon_{p_2}). \tag{25}$$

Figures 3(c) and 3(d), representing the excitation of the conduction band by two final-state electrons above the Fermi level, are also considered to be intrinsic diagrams. After a simple relabeling of final momenta, Figs. 3(c) and 3(d) are seen to be equivalent and their total contribution can be written as

$$I^i_{\mathrm{1cond}}(\epsilon_k)=\mathrm{Re}\frac{|A|^2\Delta k v_T}{\Gamma^*(\epsilon_k)(2\pi)^9}\int_{|\mathbf{p}_1|>k_F}d^3p_1\int_{|\mathbf{p}_2|>k_F}d^3p_2\int_{|\mathbf{q}|<q_c}d^3q\frac{\Theta(|\mathbf{p}_1+\mathbf{q}|-k_F)}{[\omega_p(q)+\epsilon_{p_1}+i\Sigma(p_1)-\epsilon_{|\mathbf{p}_1+\mathbf{q}|}-i\Sigma(|\mathbf{p}_1+\mathbf{q}|)]^2}$$
$$\times V(q)\omega_p(q)\delta(\epsilon_k+E_c-\omega_p(q)-\epsilon_{p_1}-\epsilon_{p_2}). \tag{26}$$

Note that in (26) we have replaced the bare energies by renormalized energies, i.e., $\epsilon_p\to\epsilon_p+i\Sigma(p)$, where $\Sigma(p)$ is the imaginary part of the self-energy on the energy shell. As indicated before,[5,12,13] without these self-energy terms this intensity function would diverge. These self-energy terms take into account higher-order interaction effects and remove divergences.

The remaining figures represent interference terms between the various processes mentioned above and are given [Figs. 3(e)–3(j)] by

$$I_1^e(\epsilon_k)=\mathrm{Re}\frac{|A|^2\Delta k v_T}{\Gamma^*(\epsilon_k)(2\pi)^9}\int_{|\mathbf{p}_1|>k_F}d^3p_1\int_{|\mathbf{p}_2|>k_F}d^3p_2\int_{|\mathbf{q}|<q_c}dq$$
$$\times\left[\mathrm{P}\frac{2\Theta(|\mathbf{p}_1+\mathbf{q}|-k_F)}{[\epsilon_k-\epsilon_{|\mathbf{k}-\mathbf{q}|}-\omega_p(q)][\epsilon_{p_1}+i\Sigma(p_1)-\epsilon_{|\mathbf{p}_1+\mathbf{q}|}-i\Sigma(|\mathbf{p}_1+\mathbf{q}|)+\omega_p(q)]}\right.$$
$$+\frac{\Theta(|\mathbf{p}_1+\mathbf{q}|-k_F)\Theta(|\mathbf{p}_2+q|-k_F)}{[\epsilon_{p_1}+i\Sigma(p_1)-\epsilon_{|\mathbf{p}_1+\mathbf{q}|}-i\Sigma(|\mathbf{p}_1+\mathbf{q}|)+\omega_p(q)][\epsilon_{p_2}+i\Sigma(p_2)-\epsilon_{|\mathbf{p}_2+\mathbf{q}|}-i\Sigma(|\mathbf{p}_2+\mathbf{q}|)+\omega_p(q)]}$$
$$\left.-\frac{2\Theta(|\mathbf{p}_1+\mathbf{q}|-k_F)}{\omega_p(q)[\epsilon_{p_1}+i\Sigma(p_1)-\epsilon_{|\mathbf{p}_1+\mathbf{q}|}-i\Sigma(|\mathbf{p}_1+\mathbf{q}|)+\omega_p(q)]}-\mathrm{P}\frac{1}{\omega_p(q)[\epsilon_k-\epsilon_{|\mathbf{k}-\mathbf{q}|}-\omega_p(q)]}\right]$$
$$\times V(q)\omega_p(q)\delta(\epsilon_k+\epsilon_c-\omega_p(q)-\epsilon_{p_1}-\epsilon_{p_2}) \tag{27}$$

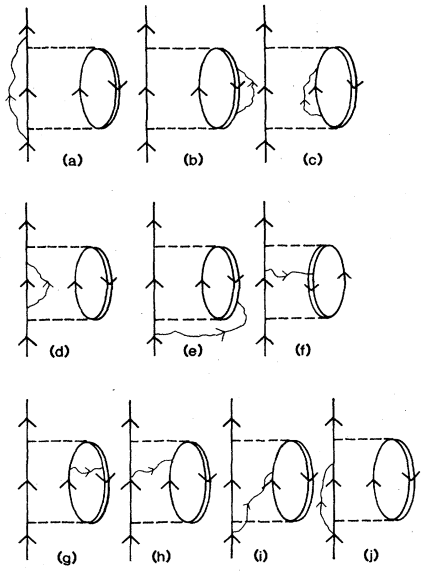

FIG. 3. Closed diagrams contributing to the APS process accompanied by one-plasmon excitation.

after some relabeling of final momenta. Note that after relabeling, $3f$ is equivalent to $3g$ and $3i$ is equivalent to $3j$. Renormalized particle energies have been used whenever the intensity function has been found to diverge.

All integrations in (24), (25), and the fourth term in (27) have been done analytically, except the one over $|\mathbf{q}|$. For (26) and the first and third terms of (27), numerical integrations have been performed over $|\mathbf{p}_1|$, $|\mathbf{q}|$, and the angle between $\mathbf{p}_1$ and $\mathbf{q}$, while an additional numerical integration over the angle between $\mathbf{p}_2$ and $\mathbf{q}$ was required for the second term in (27).

III. RESULTS AND DISCUSSIONS

Numerical computations have been carried out for the $2p$ and $1s$ APS intensity spectra of Al ($r_s=2.07$, $E_c=-61.4$ eV for L level, and $E_c=-1547$ eV for K level). Figures 4 and 5 give individual plasmon contributions to the ratio I_1/I_0 for the extrinsic, total intrinsic, and interference terms, as well as the total plasmon intensity ratio I_1^{tot}/I_0. In the presence of plasmon dispersion, the first-order diagrams are expected to show two structures in the APS spectra in simple metals.

The first is that, unlike the other terms, the extrinsic term does not begin to contribute at the plasmon threshold energy ($\epsilon_k=2E_F+\omega_p^0-E_c$). Instead, it starts to contribute at a somewhat higher energy ϵ_k at which the extrinsic process becomes real. We now calculate the minimum value of ϵ_k at which this term becomes nonzero. This process becomes real when both energy and momenta are simultaneously conserved, i.e., referring back to Fig. 2 we must have

$$\epsilon_{|\mathbf{k}-\mathbf{q}|}=\epsilon_{p_2}+\epsilon_{p_1}-E_c\ , \tag{28}$$

or solving for q,

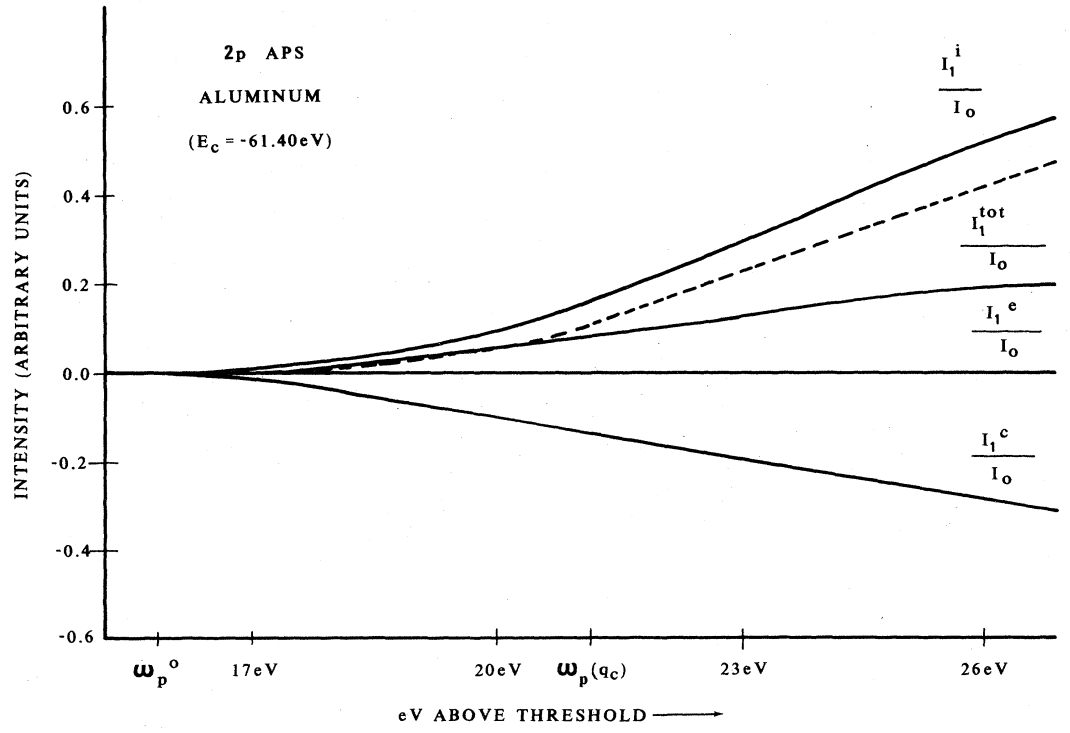

FIG. 4. Intensity ratios for the $2p$ appearance potential spectrum of Al. Total intensity is shown by the dashed curve.

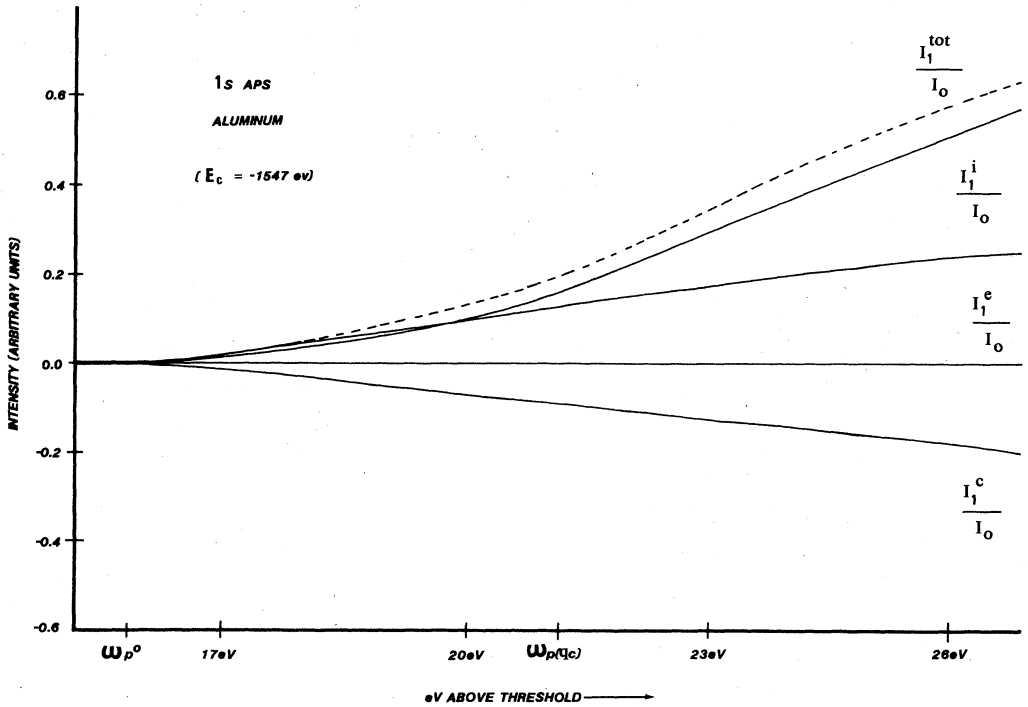

FIG. 5. Intensity ratio for the $1s$ appearance potential spectrum of Al. Total intensity is shown by the dashed curve.

$$q = k - k_F[(p_1/k_F)^2 + (p_2/k_F)^2 - E_c/E_F]^{1/2}, \quad (29)$$

this being the plasmon wave vector as a function of the other parameters. At the threshold, $|\mathbf{p}_1| = |\mathbf{p}_2| = k_F$, our q value is

$$q_T = k - k_F(2 - E_c/E_F)^{1/2}. \quad (30)$$

Conservation of total energy can be written as

$$\epsilon_k = \epsilon_{p_1} + \epsilon_{p_2} + \omega_p(q) - E_c \quad (31)$$

or at the threshold,

$$\epsilon_k = 2E_F + \omega_p[k - k_F(2 - E_c/E_F)^{1/2}] - E_c. \quad (32)$$

Solution of this transcendental equation yields the minimum value of energy of the incident electron which will excite an extrinsic plasmon. This energy obviously depends on E_c. For the L shell ($E_c = -61.4$ eV) and K shell ($E_c = -1547$ eV) this energy takes the values 16.44 and 15.81 eV above the threshold, respectively. Note that for the latter case, this energy is very close to the plasmon energy ω_p^0(15.8 eV) for Al. Figure 4 shows that at these energies the plasmon contribution from this term for the $2p$ spectrum of Al starts out smoothly with a near-zero slope. In fact, in this case close to the plasmon threshold we have found a near cancellation of all terms, as was found in the case of photoabsorption.[13] The reason for is that at these low incident energies, all processes (extrinsic, intrinsic, and interference) take place in the same spatial region resulting in a near complete cancellation of the various terms as was noted by Laramore[5] and Chastenet and Longe.[8] For the $1s$ spectrum of Al, however, the energy of the incident electron (~ 1560 eV) is not low and the cancellation is no longer complete. This fact is evident in the calculated $1s$ spectrum of Al as shown in Fig. 5, where the plasmon contribution starts with a positive slope at the threshold.

Any structures appearing in the intensity spectra are expected to become more pronounced in the derivative spectra, i.e., $dI(\epsilon_k)/d\epsilon_k$. In fact, since one observes the APS spectrum superimposed on a bremsstrahlung background, the structures in the APS are also experimentally enhanced by using the potential modulation technique, i.e., by recording $dI(\epsilon_k)/d\epsilon_k$. Thus, it is more interesting to calculate the derivative of the intensity. We have carried out a numerical computation of the derivative of the $2p$ and $1s$ APS intensities for Al and the results are shown in Figs. 6 and 7, respectively.

As expected, the above-mentioned structure at the plasmon threshold ($\epsilon_k \approx 2E_F + \omega_p^0 \approx 15.8$ eV above threshold) becomes more pronounced in the $1s$ derivative spectrum of Al (Fig. 7). However, for reasons discussed above there is only slight modulation at the corresponding energy in the $2p$ derivative spectrum (Fig. 6).

A second structure occurs in both $1s$ and $2p$ derivative spectra at the frequency corresponding to the plasmon cutoff frequency $\omega_p(q_c)$ (≈ 21.2 eV $> \omega_p^0$) above the APS threshold. This structure is brought about by the processes which correspond to the excitation of a plasmon by the two final-state electrons shown in Figs. 2(c) and 2(d). The reason for this structure at this energy is that this is the lowest value of ϵ_k where the plasmon excitation becomes real. The same result occurs for the x-ray photoabsorption case, and the reader should refer to Ref. 13 for a de-

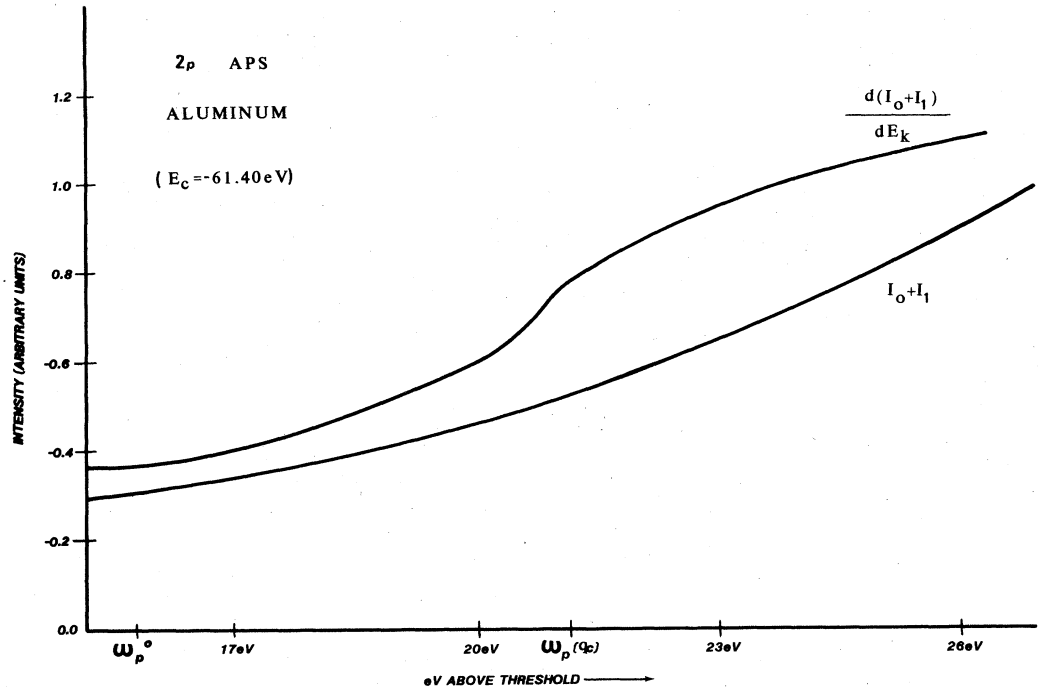

FIG. 6. Derivative $2p$ appearance potential spectrum of Al. Note that there is a change in concavity at incident electron energy $2E_F+\omega_p(p_c)-E_c$ (=21.2 eV above threshold).

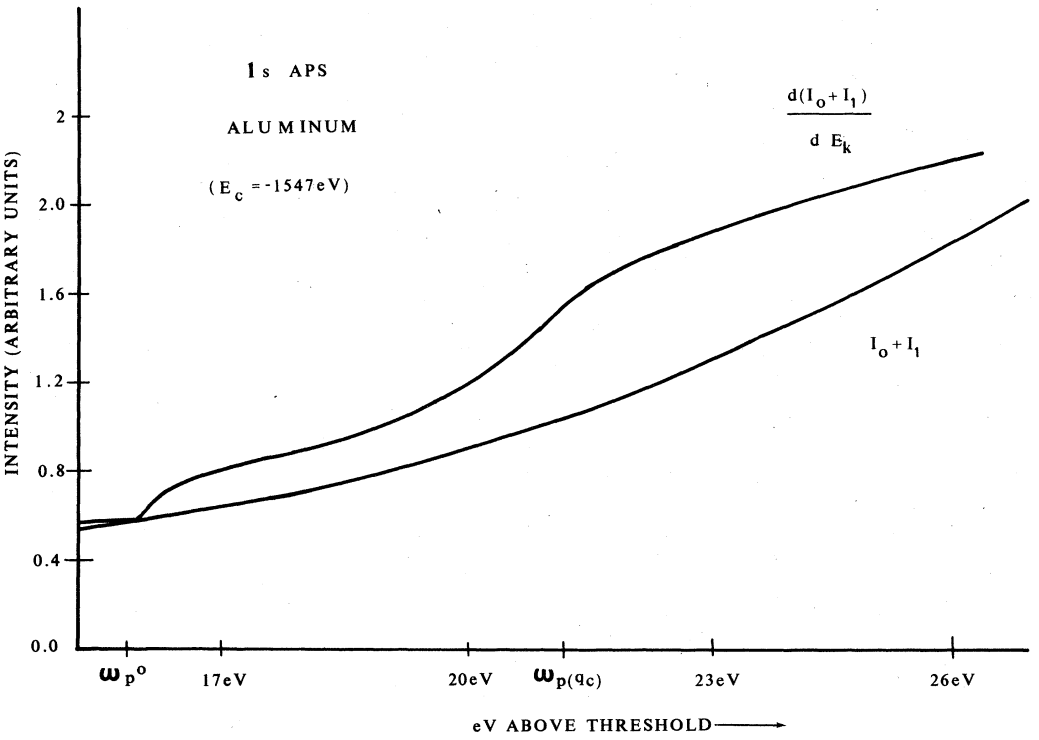

FIG. 7. Derivative $1s$ appearance potential spectrum of Al. Note that there are two structures present in this spectrum: one in the form of a steep rise at $2E_F+\omega_p^0-E_c$ (=15.8 eV above threshold) and the other a change in concavity at $2E_F+\omega_p(q_c)-E_c$ (=21.2 eV above threshold).

tailed discussion regarding the origin of this structure. As can be seen in Figs. 6 and 7, this structure appears as a change in slope in both $1s$ and $2p$ derivative spectra of Al.

In the experimental $2p$ derivative spectrum of Al by Nilsson and Kanski,[3] no significant structure has been observed at an energy corresponding to the plasmon threshold energy ω_p^0. This agrees with our calculation that no major structure is expected at this energy because of near-complete cancellation of the various terms contributing to the plasmon satellite. However, in this experimental $2p$ spectrum, a structure is present at approximately 21 eV above the threshold. It can be identified with the structure we have calculated in this paper (see Fig. 6) at $\omega_p(q_c)$ above the threshold, even though it has traditionally been attributed to the peak calculated near this energy in the density-of-states function of Al.[14] The experimental $1s$ derivative spectrum $dI(\epsilon_k)/d\epsilon_k$ of Andersson and Nyberg[2] of Al is somewhat different. In this case a pronounced peak is observed around 15.5 eV above the threshold, which can be identified with the threshold plasmon structure we have calculated at this energy (Fig. 7). A careful study of this experimental derivative spectrum indicates that there is a hump near 21 eV above the threshold. This hump may be associated with the second plasmon structure we have calculated at this energy in the $1s$ derivative spectrum of Al.

In conclusion, in this paper we have studied the plasmon bands in the $1s$ and $2p$ APS spectra of Al. We have calculated two structures in the $1s$ spectrum, near 15 and 21 eV above the threshold, and in the $2p$ spectrum one structure near 21 eV above the threshold. These theoretical results appear to be verified by the presently available experimental spectra. However, as there are other structures present in the APS spectra of simple metals due to band structure and extended fine-structure effects, it would be useful if further experiments were performed for more positive identification of the plasmon structures calculated in this paper. Finally, it is interesting to note that since the structures are expected to appear at the threshold and cutoff of plasmon energy, their positive identification will give an experimental estimation of the extent of plasmon dispersion in metals.

ACKNOWLEDGMENT

One of the authors (P.L.) is grateful to Fonds National de la Recherche Scientifique, Belgium and the Cooperation Scientifique Internationale, Belgium, for financial support.

[1]J. E. Houston and R. L. Park, Solid State Commun. **10**, 91 (1979).
[2]A. Andersson and C. Nyberg, Solid State Commun. **28**, 803 (1978).
[3]P. O. Nilsson and J. Kanski, Surf. Sci. **37**, 700 (1973).
[4]J. J. Chang and D. C. Langreth, Phys. Rev. B **5**, 3512 (1972).
[5]G. E. Laramore, Solid State Commun. **10**, 85 (1972).
[6]A. J. Glick and R. A. Ferrell, Ann. Phys. (N.Y.) **11**, 359 (1960).
[7]S. M. Bose, A. Bardasis, A. J. Glick, D. Hone, and P. Longe, Phys. Rev. **155**, 379 (1967).
[8]D. Chastenet and P. Longe, Phys. Rev. Lett. **44**, 91 (1980).
[9]S. M. Bose, P. Kiehm, and P. Longe, Phys. Rev. B **23**, 712 (1981).
[10]D. Pines, *Elementary Excitations in Solids* (Benjamin, New York, 1963).
[11]L. I. Schiff, *Quantum Mechanics,* 3rd ed. (McGraw-Hill, New York, 1968).
[12]J. Fitchek, R. Patrick, and S. M. Bose, Phys. Rev. B **26**, 6390 (1982).
[13]S. M. Bose and P. Longe, Phys. Rev. B **18**, 3921 (1978).
[14]J. W. D. Connolly, Intern. J. Quantum Chem. III S, 807 (1970).